# Final Report

# LOW FLUXES OF X-RAYS



February 1976



TELEDYNE
BROWN ENGINEERING

Cummings Research Park • Huntsville, Alabama 35807

FINAL REPORT
MS-MSFC-1975

# LOW FLUXES OF X-RAYS

February 1976

Prepared For

SPACE SCIENCES LABORATORY
GEORGE C. MARSHALL SPACE FLIGHT CENTER
MARSHALL SPACE FLIGHT CENTER, ALABAMA

Contract No. NAS8-26342

Prepared By

SYSTEMS ANALYSIS DEPARTMENT
MILITARY SYSTEMS
TELEDYNE BROWN ENGINEERING
HUNTSVILLE, ALABAMA

ABSTRACT

Analytic and experimental investigations of the interactions of high-energy protons with spacecraft materials and light nucleus atoms have been conducted. Irradiation of typical materials for scintillation detectors using accelerator-produced energetic protons and associated theoretical calculations indicate activity within detectors produced by this mechanism is significant to detection of low-level cosmic gamma radiation. Samples of several materials were flown aboard Skylab to obtain measures of the neutron and proton flux environment. Extremely weak activity was produced in the samples. Calculations of interactions of intermediate-energy protons with light nuclei were performed and a more complete theoretical model programmed for digital computation. Preliminary results appear promising for calculating products of such interactions, but additional work remains to be done.

Approved

N. E. Chatterton, Ph.D.
Manager, Research

W. A. Grenard
Manager, Systems Analysis Department

TABLE OF CONTENTS

## LIST OF ILLUSTRATIONS

LIST OF TABLES

# 1. INTRODUCTION

This report synopsizes the results of a series of investigations, both analytic and experimental, of the effects of the radiation environment on Earth-orbital and balloon-borne systems and a study of cosmic sources of relatively high-energy photon radiation.

The radiation environment was considered for its importance inducing radioactivity in such a manner as to affect the capabilities of radiation detectors designed to study distant low-level gamma-ray sources. This radioactivity can be induced in the structural materials of the measurement platform, the atmosphere (for balloon-borne measurement systems), or in the detector material itself.

Both the early and late work performed on this contract has been dedicated to theoretical analyses of reaction cross-sections. The earlier results were documented previously; this document provides a summary of the latest work.

Another portion of the work was directed toward a combined experimental and computational program of investigation of induced radioactivity determination. Radioactivity induced by protons in sodium iodide scintillation crystals was calculated and measured directly. These data are useful in determining trapped radiation and cosmic-ray-induced background counting rates in space-borne detectors. Neutron- and proton-induced radioactivity at various locations within Skylab was measured. Low-level gamma-ray spectroscopy measurements were made on the returned samples to determine the incident neutron and proton fluxes and spectra and their variations with mass distribution.

Teledyne Brown Engineering also contributed to the design of a balloon-borne gamma-ray measurement apparatus and the construction and checkout of the apparatus and its use for astronomical measurements.

# 2. EARLY THEORETICAL WORK

A summary of the status of the problem of describing high-energy nuclear reactions including descriptions of specific models to predict observed phenomena was presented (Ref. 1). This work was extended in the last few months and formed the basis of the experimental work that followed the original analysis. A more complete description of the analysis and recent modeling work are presented in Section 4 of this report.

# 3. INVESTIGATION OF INDUCED RADIOACTIVITY

## 3.1 STUDIES OF INDUCED RADIOACTIVITY IN DETECTORS

Proton-induced radioactivity of scintillation detectors is an important source of background counting rate whenever these detectors are used in a space environment. In addition to the ever-present primary cosmic-rays penetrating spacecraft in Earth orbit, the trapped proton radiation adds considerably to the total proton flux. For orbits of low altitude and medium inclination, the largest fraction of proton flux is received in the region of the South Atlantic Anomaly. Figure 3-1 shows the flux contours for protons with energies greater than 5 MeV at an altitude of 600 kilometers (Ref. 2). Figure 3-2 gives the proton energy spectrum averaged over 24 hours for an orbit at an altitude of 720 kilometers and an inclination of 30 degrees (Ref. 3). Figure 3-3 gives the primary cosmic-ray spectrum near the Earth.

Radioactivity induced in spacecraft scintillation detectors was first recognized and analyzed by Peterson on his OSO 1 experiment (Ref. 4). The analysis of data from the Russian gamma-ray experiments on the Cosmos 135 and Cosmos 163 spacecraft has included corrections for the radioactivity induced by passage through the region of the South Atlantic Anomaly, although the details of these corrections have not been given (Ref. 5). Dyer and Morfill (Ref. 6) have calculated the induced radioactivity in CsI(Tℓ) by the same general method used by Fishman (Ref. 7) and have compared these calculations to radioactivity induced by 155-MeV protons. This energy is representative of that of nuclear-interacting trapped protons. Their measurements are used in a study of the anticipated background radiation on the UK-5 celestial gamma-ray experiment. The data contained within Reference 7 have been used to determine the effect of cosmic-ray-induced radioactivity on diffuse celestial gamma-ray measurements (Ref. 8).

To deduce the amount of radioactivity and its energy and time decay spectrum induced in scintillation detectors by protons, both an analytical approach and an experimental approach were undertaken. The

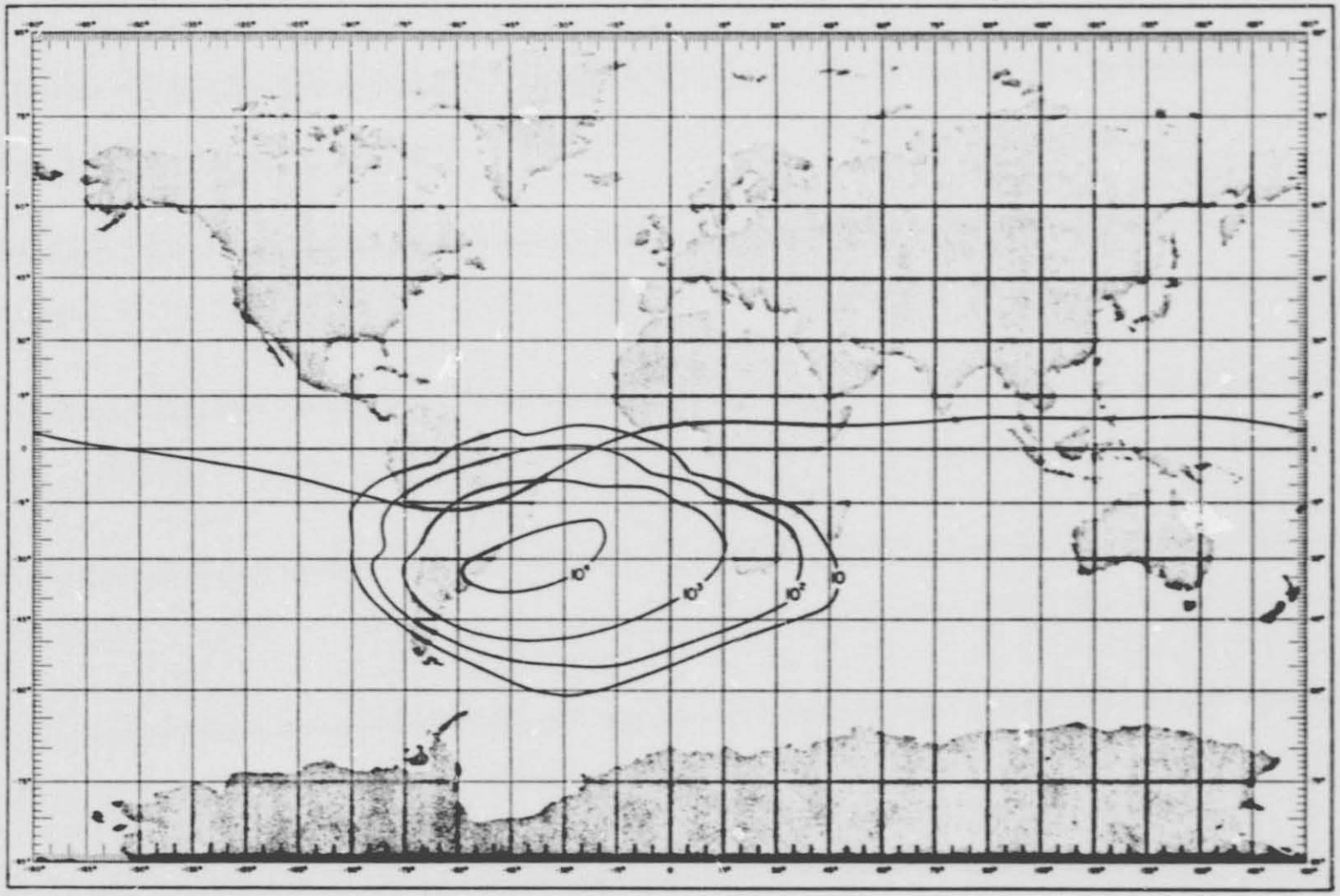

ALTITUDE = 600 km

FIGURE 3-1. PROTON FLUX CONTOURS FOR $E_p$ > 5 MeV

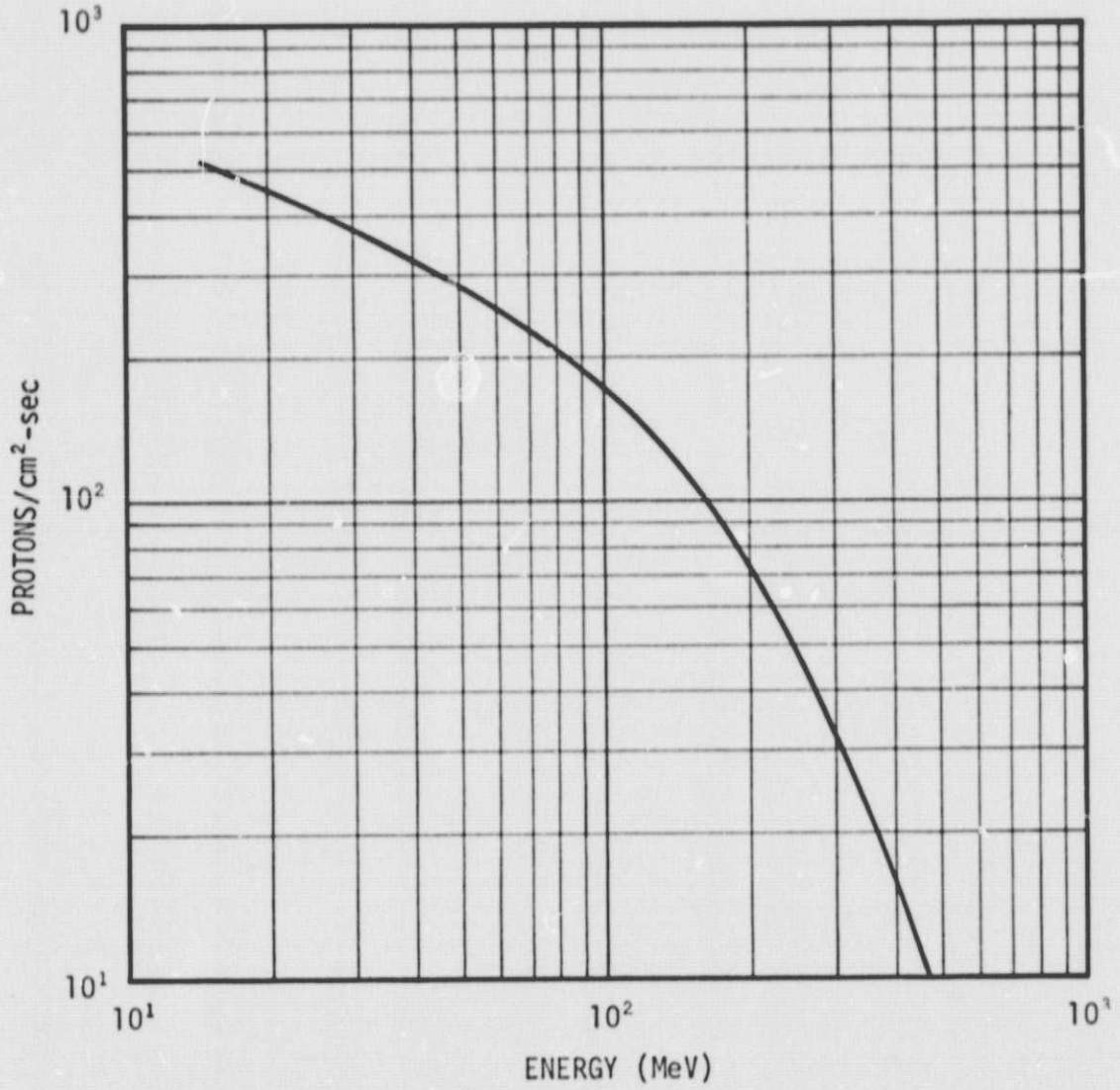


FIGURE 3-2. PROTON ENERGY SPECTRUM FOR h = 720 km, i = 30 degrees

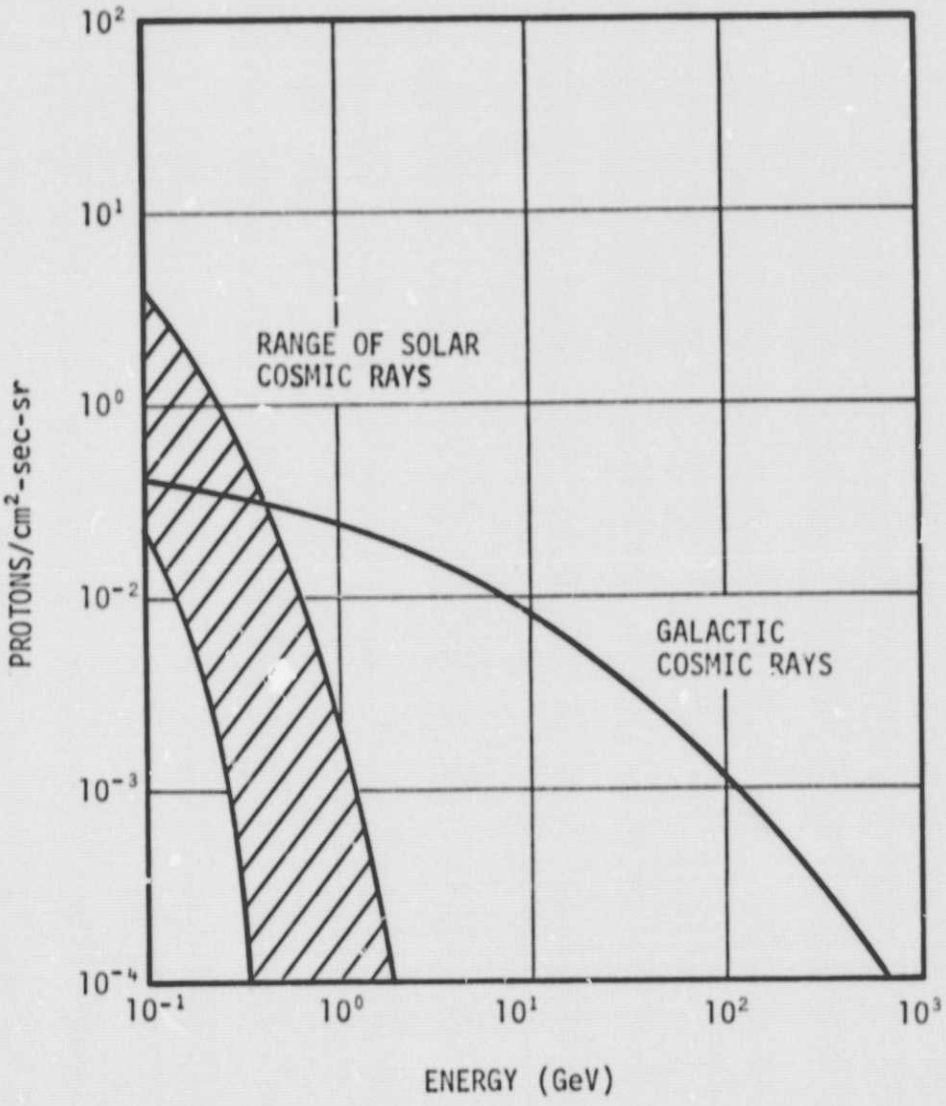


FIGURE 3-3. PRIMARY GALACTIC AND SOLAR COSMIC-RAY SPECTRA

analytical approach consisted of calculations of spallation yields and a study of the nuclear properties of the spallation products. The experimental approach was to irradiate a scintillation detector with high-energy protons and directly observe the counts resulting from the decay of induced radioactivity. Both approaches are limited in their estimation of the radioactivity induced in a true space environment. However, within errors, both estimates were in agreement and may prove useful in design and data reduction applications for space-borne experiments using scintillation detectors.

Calculations of spallation yields were made for protons interacting with sodium iodide at energies above 100 MeV using the semi-empirical formulas derived by Rudstam (Ref. 9). These formulas give the cross section for spallation production within a factor of three over a wide range of atomic mass numbers and incident proton energies.

In an effort to measure directly the radioactivity induced in a scintillation detector, an accelerator experiment was performed at the NASA Space Radiation Effects Laboratory, Newport News, Virginia. A sodium iodide detector, 17 gm-cm$^{-2}$ thick, was irradiated with a low flux of 600-MeV protons over a 10-second period. The integrated irradiation flux, $7 \times 10^{10}$ protons in a 5-centimeter-diameter sodium iodide detector, was measured using the known cross section for the $I^{127}$ (p, p 4n) $I^{123}$ reaction as a beam monitor (Ref. 10). The number of $I^{123}$ nuclei produced were derived from the 0.192-MeV line observed in the decay spectrum at a known time after the irradiation. Continuum and background radiation corrections were made to the data in this derivation; however, the accuracy of the data is estimated at only ±30 percent because of the magnitude of the corrections and the uncertainty of the $I^{123}$ cross section.

Counting rate spectra were taken at various times after the irradiation. In general, the spectra show exponential continua with several discrete peaks superimposed. Most of the peaks from electron capture and internal transition decays of radioactive isotopes of iodine, tellurium, and antimony could be identified in the spectra. The continuous

nature of the spectra arises from the large number of radioactive products involved and the fact that most transitions include a non-discrete beta transition.

The study indicated that proton-induced radioactivity will be a major source of background radiation for low-level, space-borne detectors in the hard X-ray and gamma-ray regions. Approximately one gamma-ray will be produced after each nuclear interaction. The decay of the induced radioactivity will roughly follow a 1/t rate, and the energy spectrum is expected to be exponential with an e-folding energy of approximately 0.9 MeV. Proton irradiation data at 600 MeV are in agreement with the above results.

More precise calculations may be made using experimental cross section data and detailed decay schemes. The actual proton transport within heavy spacecraft will be needed for these calculations, along with the proton dose history.

## 3.2 STUDIES OF INDUCED RADIOACTIVITY IN SPACECRAFT MATERIALS

Large, orbiting spacecraft are expected to produce significant numbers of neutrons through nuclear reactions between trapped protons and spacecraft materials. Although measurements of upward-moving atmospheric neutrons (the neutron albedo) have been made, locally produced, secondary neutrons in spacecraft have not yet been studied. Secondary neutrons have previously been shown to contribute a negligible dose to astronauts, but their great penetrating power and ability to activate many materials may seriously degrade the sensitivity of X-ray and gamma-ray detectors on orbiting spacecraft. This is especially true of scintillation and solid-state detectors aboard the High-Energy Astronomy Observatory spacecraft. For these detectors, prompt, charged-particle-produced background can be greatly reduced by active shielding, whereas there is no known method of reducing activation background in the detectors.

The Skylab Neutron Environment Science Demonstration measured neutrons and protons by the activation analysis technique (Ref. 11). In this technique, samples of known composition were exposed to the unknown neutron and proton environment at various locations within Skylab. After return of the samples, they were analyzed in a low-level, high-resolution gamma-ray spectrometer to deduce the type and amount of radioactive isotopes produced during their irradiation. The neutron and proton environments can then be derived by using the appropriate activation cross sections.

Four activation sample packets were flown and returned on the Skylab IV mission. They were deployed by the crew at the locations within the Orbital Workshop (OWS) given in Table 3-1. The four activation sample packets each contained five samples of high-purity metals, with dimensions of 1.91 by 1.91 by 0.32 centimeters. Four of the metal samples were tantalum, nickel, titanium, and hafnium. The fifth sample was tantalum with a covering layer of 0.65-millimeter-thick cadmium, which excluded thermal neutrons. The cadmium had a minimum absorption length of seven mean-free paths for neutrons with energies less than 0.2 eV. The samples were sewn into beta cloth (fiberglass) to form the activation packets. Table 3-2 indicates the properties of the samples.

The activation packets were in the Skylab IV orbit for the mission duration (November 14, 1973, to February 5, 1974). During the initial 5.3 days and the final 2.7 days of the mission, the packets were stowed in a Command Module locker. The remainder of the time, 76.0 days or 91 percent of the orbital time, the packets were deployed at the locations given in Table 3-1.

The radioactive isotopes found in the returned samples, along with their nuclear decay properties and production modes, are listed in Table 3-3. All activities found were extremely weak; the average count rate for a particular isotope was less than one count per hour.

TABLE 3-1. ACTIVATION PACKET LOCATIONS

| PACKET | LOCATION | SHIELDING -- RADIATION ENVIRONMENT EXPECTED |
|---|---|---|
| 1-FV | OWS Film Vault, Drawer J | Maximum shielding -- secondary neutrons, few protons |
| 2-WT | Water Storage Tank (Full), OWS, Taped on Outside of Tank | Moderate shielding -- thermalized neutrons |
| 3-OWS FWD | OWS Forward -- Taped on Domed Bulkhead | Average shielding -- near center of mass of Skylab cluster |
| 4-OWS AFT | OWS Aft -- Taped on Outside Wall in Sleep Compartment | Minimum shielding for internal location -- few secondary neutrons, maximum protons |

TABLE 3-2. ACTIVATION SAMPLES

| SAMPLE | NOMINAL WEIGHT (grams) | MAIN ISOTOPES |
|---|---|---|
| 1. Tantalum (bare) | 19 | $Ta^{181}$ (100%) |
| 2. Tantalum (cadmium-wrapped) | 19 | $Ta^{181}$ (100%) |
| 3. Nickel | 12 | $Ni^{58}$ (68%), $Ni^{60}$ (26%) |
| 4. Titanium | 5.6 | $Ti^{48}$ (74%), $Ti^{46}$ (8%), $Ti^{47}$ (7%) |
| 5. Hafnium | 17 | $Hf^{180}$ (35%), $Hf^{179}$ (14%), $Hf^{178}$ (27%), $Hf^{177}$ (19%) |

TABLE 3-3. ACTIVATION ISOTOPES IDENTIFIED

| ISOTOPE | $\tau_{1/2}$ (DAYS) | $E_\gamma$ (keV) | PRODUCTION MODES | |
|---|---|---|---|---|
| | | | MAIN | OTHER |
| $Co^{58}$ | 71 | 810 | $Ni^{58}(n,p)$ | Ni(p,2pxn), Ni(n,pxn) |
| $Ta^{182}$ | 115 | 1121<br>1189<br>1222<br>1231 | $Ta^{181}(n,\gamma)$ | |
| $Co^{56}$ | 77 | 847 | $Ni^{58}(p,2pn)$ | Ni(p,2pxn), Ni(n,pxn), Ni(p,pxn)$Ni^{56}$, Ni(n,xn) $Ni^{56}$ |
| $Co^{57}$ | 270 | 122 | $Ni^{58}(p,2p)$ | Ni(p,2pxn), Ni(n,pxn), Ni(n,xn)$Ni^{57}$ |
| $V^{48}$ | 16 | 983 | $Ti^{48}(p,n)$ | |
| OTHER IDENTIFICATIONS (WEAK) | | | | |
| $Sc^{46}$ | 84 | 889 | Ti(p,-) | |
| $Lu^{171}$ | 8.3 | 741 | Hf(p,-) | Ta(p,-) |
| $Hf^{175}$ | 70 | 343 | Hf(p,-) | Ta(p,-) |

The preliminary measurements showed that both neutron and proton activation isotopes were produced in the samples from which several qualitative observations can be made:

- $Co^{58}$, which has a high-yield cross section from $Ni^{58}$ via the fast neutron (n, p) reaction, is produced in greater quantity in the higher mass locations.
- $Co^{56}$ and $V^{48}$, which are proton activation products of nickel and titanium, respectively, are produced at the lower mass locations. $Co^{57}$ shows no clear enhancement.
- $Ta^{182}$, a neutron capture product, is produced more at the higher mass locations. The capture cross section rises rapidly at thermal neutron energies. The lack of enhancement at the water tank location probably indicates a low thermal to fast neutron flux ratio. Measurements of the cadmium-wrapped tantalum, not made under this contract, should indicate the thermal neutron component.
- Proton activation in the film vault location, as evidenced by $Co^{56}$ and $V^{48}$, indicates the presence of the high-energy tail of trapped protons and/or primary galactic cosmic rays. Some of this activation could be due to temporary storage of the packet while in the Command Module.

Reference 11 contains more complete information on this experiment.

# 4. RECENT THEORETICAL TREATMENT

## 4.1 INTRODUCTION

Charged particles, protons, and alpha particles, and in some cases light nuclei such as $_6C^{12}$ and $_8O^{16}$, are effective tools to study nuclear structure by investigating the reaction products with target nuclei in various mass ranges. In particular, proton reactions with selected light nuclei such as $_6C^{12}$, $_7N^{14}$, $_8O^{16}$, and $_{10}Ne^{20}$ are of considerable interest because of the abundance of these nuclei in the upper atmosphere. Reactions with these nuclei by protons occurring in cosmic radiation in the upper atmosphere are of concern for balloon-borne measurement apparatus. Of particular interest are proton reactions with light nuclei for proton energies ranging from 10 to 20 MeV. It is of interest to investigate the mechanisms of these types of reactions by developing an appropriate formalism and to study the gamma-ray production cross section as a function of the incident proton energy. The most recent work on this contract was again addressed to the problem of these computations.

## 4.2 THEORETICAL MODEL

### 4.2.1 Types of Reactions

When a charged particle such as a proton approaches a nucleus with energies low compared with the Coulomb barrier exhibited by the target nucleus under consideration, the particle interacts only with the Coulomb field, and this leads to ordinary elastic scattering. As the energy of the incident proton increases, it begins to interact with the nuclear field so that the approaching particle can be either elastically scattered or absorbed to form a compound nucleus. If a compound nucleus is formed, this intermediate nucleus will be in an excited state from which de-excitation will take place either by emitting a proton with energy equal to that of the incident proton or by emitting a proton of energy different from - usually less than - that of the incident proton. The former type of reaction is called a compound elastic reaction, and the latter is called a compound inelastic reaction. In the compound inelastic

reaction, the difference in energy between the incident and emitted proton is left in the residual nucleus, leaving it in an excited state; it de-excites through gamma-ray emission until it reaches its ground state. However, if the incident proton energy is sufficiently large, then the compound state can be followed by particle emission leading to a residual nucleus different from the target or the compound nucleus. The residual nucleus is generally left in an excited state, and this emission of a particle different from the projectile particle leads to a de-excitation mechanism, which could open various channels of particle and gamma-ray emission. If the original reaction leads to emission of more than one particle, the mechanism is rather complicated and a simple approach to this aspect of the problem is not possible.

In addition to elastic and compound nucleus reactions, a third type of reaction that can take place is the direct reaction. In the case of direct reactions, the intermediate compound nuclear state is not formed; instead, the projectile reacts directly with the target nucleus, leading to inelastic (p,p') scattering or pickup or charge exchange reactions. A typical pickup reaction is (p,d), and a similar charge exchange reaction is (p,n). These different types of reactions are represented schematically in Figure 4-1.

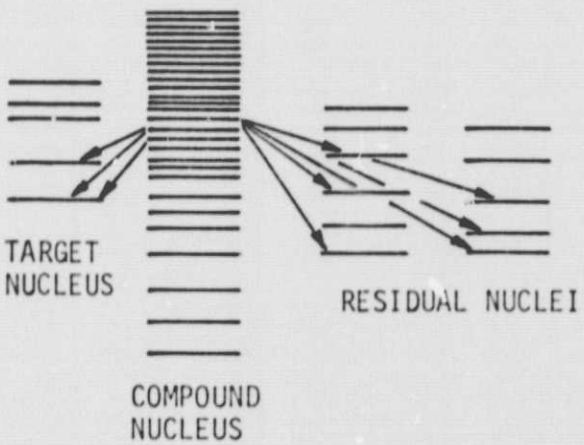


FIGURE 4-1. COMPOUND NUCLEUS ENTRANCE AND EXIT CHANNELS

### 4.2.2 Elastic Scattering

The theory of elastic scattering is very well worked out and is rather well understood. However, for the sake of completeness, a brief outline of the theory is described here. The reaction mechanism of a spinless neutral particle is discussed first so that the discussion of charged particle reactions can be understood better. The Schrödinger equation for such a reaction can be written as

$$\nabla^2 \psi + \frac{2m}{\hbar^2} [E - V(r)] \psi = 0. \qquad (4\text{-}1)$$

The solution for this must satisfy, for large r, an incident plane wave and a scattered spherical wave.

Assuming that the particle is approaching the target nucleus in the Z direction, one can write the asymptotic form of the wave function in spherical coordinates as

$$\psi \sim \exp(ikz) + \frac{\exp(ikr)}{r} f(\theta) , \qquad (4\text{-}2)$$

where

$$k = \frac{\sqrt{2mE}}{\hbar} ,$$

m is the mass of the projectile, and E is its energy. The problem is to calculate $f(\theta)$ for an appropriate potential. To do this, one attempts to solve Equation 4-1 by expanding the wave function $\psi$ into a product of radial and angular parts and writes

$$\psi = \sum_{\ell} \frac{U_\ell(r)}{r} P_\ell(\cos\theta) , \qquad (4\text{-}3)$$

where $\ell = 0, 1, 2 \ldots$ represents the orbital angular momentum quantum number and $P_\ell(\cos\theta)$ are ordinary Legendre polynomials.

When $\psi$ as given in Equation 4-3 is substituted into Equation 4-1, Equation 4-1 will lead to

$$\frac{d^2 U_\ell}{dr^2} + \left[\frac{2m}{\hbar^2}(E - V) - \frac{\ell(\ell+1)}{r}\right] U_\ell = 0. \qquad (4\text{-}4)$$

The angular part disappears and it is only the radial part that appears in Equation 4-4. To make matters simpler, one at this stage looks into s-wave scattering, which immediately reduces Equation 4-4 to a simple form since $\ell$ is set equal to zero. Thus,

$$\frac{d^2 U_0}{dr^2} + \frac{2m}{\hbar^2}(E - V) U_0 = 0$$

or

$$\frac{d^2 U}{dr^2} + k^2 U_0 = 0. \qquad (4\text{-}5)$$

Obviously, Equation 4-5 has a solution of the form

$$U_0 = A \sin(kr + \delta)$$

$$= A \exp(-i\delta)\,[\exp(2i\delta)\exp(ikr) - \exp(-ikr)]. \qquad (4\text{-}6)$$

However, from Equation 4-3 for s-wave scattering, one obtains, since $P_0(\cos\theta)$ is equal to unity, the relation

$$\psi = \frac{U}{r}. \qquad (4\text{-}7)$$

Therefore, for $\ell = 0$

$$U = r(\psi^0_{in} + \psi^0_{out}), \qquad (4\text{-}8)$$

where $\psi_{in}$ gives the incident wave and $\psi_{out}$ gives the scattered wave. However, by the assumption made in Equation 4-2, the incident wave will be given by

$$\psi_{in} = \exp(ikz). \qquad (4\text{-}9)$$

For s-wave scattering, this can be determined from the expansion of Equation 4-9 into a combination of Bessel functions and Legendre polynominals and by setting $\ell$ to zero in the expansion obtained. This leads to

$$\exp(ikz) = \sum_{\ell=0}^{\infty} (2\ell + 1)\, i^{\ell}\, j_{\ell}(kr)\, P_{\ell}(\cos\theta), \qquad (4\text{-}10)$$

so that for s-wave scattering Equation 4-10 can be rewritten, by making use of the expansion of Bessel functions and also by remembering $P_0(\cos\theta)$ is unity, as

$$\exp(ikz)\ (\ell = 0) = \frac{\sin kr}{kr} \qquad (4\text{-}11)$$

or

$$\exp(ikz)\ (\ell = 0) = \frac{1}{2ikr}\ [\exp(ikr) - \exp(-ikr)]\ . \qquad (4\text{-}12)$$

From physical considerations, it is obvious that the scattered wave is given by

$$\psi_{out}\ (\ell = 0) = \psi - \psi_{in}\ (\ell = 0)\ . \qquad (4\text{-}13)$$

At this stage, one uses the solution of the Schrödinger equation as given in Equation 4-6, the relation given in Equation 4-7, and Equation 4-12 to obtain

$$\psi_{out}\ (\ell = 0) = \frac{A \exp(-i\delta)}{2i}\ [\exp(2i\delta)\exp(ikr) - \exp(-ikr)]$$

$$- \frac{1}{2ikr}\ [\exp(ikr) - \exp(-ikr)]. \qquad (4\text{-}14)$$

Again, the physical condition requires that the outgoing wave should contain no exp (-ikr) term, and this condition can be satisfied in Equation 4-4 by setting the terms containing exp (-ikr) to add up to zero. Such a restriction leads to

$$- \frac{A \exp(-i\delta)}{2i} \exp(-ikr) + \frac{1}{2ikr} \exp(-ikr) = 0 \qquad (4\text{-}15)$$

or

$$\frac{A \exp(-i\delta)}{2i} = \frac{1}{2ikr} \quad . \qquad (4\text{-}16)$$

One uses the result obtained from Equation 4-16 in Equation 4-14 to reduce it to

$$\psi_{out} (\ell = 0) = \frac{2}{2ikr} [\exp(2i\delta) - 1] \exp(ikr). \qquad (4\text{-}17)$$

By comparing Equation 4-17 with Equation 4-2, one can conclude that

$$f(0)_{\ell=0} \sim \frac{1}{2ik} [\exp(2i\delta) - 1]. \qquad (4\text{-}18)$$

Differential scattering cross section is defined as the square of the amplitude of the scattered wave, which, from Equation 4-2, becomes

$$\frac{d\sigma}{d\Omega} = |f(0)|^2 \quad . \qquad (4\text{-}19)$$

The value of this is determined by making use of Equation 4-18. Of course this will give only the value for the s-wave scattering. However, using a similar approach, one can evaluate the cross section for p-wave ($\ell$=1) or higher-order scattering cross sections.

### 4.2.3 Compound-Nucleus Formation and Hauser-Fesbach Formalism

The discussion in the previous section of shape elastic scattering now leads to compound-nucleus reaction as the next problem in sequence to be confronted. The simplest type of compound-nucleus reaction is the one in which no direct reactions exist in the nonelastic channels, and in such a case a statistical approach is valid. As in the case of elastic scattering, it is convenient to discuss the reaction from one initial state to one final state in the absence of spin. The details of the

formalism have been worked out by Hauser and Feshach and also extensively discussed in the literature. Therefore, the salient aspects of the theory will be briefly discussed.

Let α denote the initial state and β denote the final state, and let the spins of the entrance channel be denoted by ℓ and s and similar quantities for the exit channels by ℓ' and s'. Here, s denotes the vector sum of the spin of the projectile and target nucleus and s' denotes the same for the residual nucleus and the emitted particle. Thus, one can write

$$s + \ell = s' + \ell' \tag{4-20}$$

from conservation of angular momentum.

The compound nucleus can decay elastically, in which case the emitted particle is identical to the projectile. In the terminology above, this implies that

$$\alpha = \beta.$$

The scattering matrix, S, in this case will be diagonal. As before, if one begins by considering the reaction in the case of spinless particles, the cross section for the formation of the compound nucleus can be shown to be

$$\sigma_{\alpha\beta} = \pi \lambda_\alpha^2 \left\langle |\delta_{\alpha\beta} - S_{\alpha\beta}|^2 \right\rangle \ , \tag{4-21}$$

where $S_{\alpha\beta}$ is the scattering matrix. The cross section for the formation of a compound state leading to an emission back into the entrance channel, which implies compound elastic scattering, may be obtained from Equation 4-21, where $\delta_{\alpha\beta} \equiv 1$, leading to

$$\sigma_{\alpha\alpha} = \pi \lambda_\alpha^2 \left(1 - 1\ S_{\alpha\alpha}|^2\right)$$

$$= \pi \lambda_\alpha^2\ T_\alpha \ . \tag{4-22}$$

In Equation 4-22, $T_\alpha$ is the transmission coefficient. Transmission coefficients can be calculated by using an appropriate optical potential. In the nonelastic case, one is interested in $\sigma_{\alpha\beta}$, and to evaluate this it is necessary to determine $|S_{\alpha\beta}|^2$. The standard technique used is to apply the physical principle that the formation and decay of the compound state are independent of each other so that one can write

$$\left\langle |S_{\alpha\beta}| \right\rangle = \left\langle |S_{\hat{\alpha}\hat{\beta}}| \right\rangle \ , \tag{4-23}$$

which is equivalent to stating that

$$\lambda_\alpha^2 \, \sigma_{\alpha\beta} = \lambda_\beta^2 \, \sigma_{\hat{\alpha}\hat{\beta}} \ .$$

If the probability of decaying into channel $\beta$ is designated by $P_\beta$, then Equation 4-21 can be written as

$$\begin{aligned} \sigma_{\alpha\beta} &= \sigma_\alpha^{CN} \, P_\beta \\ &= \pi \lambda^2 \, T_\alpha \, P_\beta \ . \end{aligned} \tag{4-24}$$

Following the theoretical formalism of Hauser and Feshach, the probability of the formation of a compound nucleus of spin J from channel $\alpha$ is (from Equations 4-22, 4-23, and 4-24):

$$T_\alpha \, P_\beta = T_{\hat{\alpha}} \, P_{\hat{\beta}} \ . \tag{4-25}$$

This statement is true for all possible channels $\alpha$ and $\beta$. One can conclude, from Equation 4-25, that

$$\frac{P_{\hat{\alpha}}}{T_\alpha} = \frac{P_{\hat{\beta}}}{T_\beta} = \lambda \ , \tag{4-26}$$

where $\lambda$ is a constant. Obviously, the probabilities hold the relationship

$$\sum_\alpha P_\alpha = \sum_\beta P_\beta = 1$$

and

$$\sum_{\alpha} P_{\alpha} = \lambda \sum_{\alpha} T_{\alpha} = 1. \tag{4-27}$$

Thus, it is readily seen that

$$P_{\beta} = \lambda T_{\hat{\beta}} = \frac{T_{\hat{\beta}}}{\sum_{\alpha} T_{\alpha}} . \tag{4-28}$$

Since the compound nucleus can decay back into the incident channel, the summation in Equation 4-28 has to be over the incident and all the outgoing channels. Thus, combining Equations 4-24 and 4-28 yields

$$\sigma_{\alpha\beta} = \pi \lambda^2 \frac{T_{\alpha} T_{\hat{\beta}}}{\sum_{i} T_{i}} . \tag{4-29}$$

Equation 4-29 is essentially the Hauser-Fesbach formula for the case of spinless particles. The generalization of Equation 4-29 requires the introduction of the spins of the channels involved. Let i denote the spin of the incident particle, I the spin of the target nucleus and $j = I + i$ the incident channel spin, and $j' = I' + i'$ the corresponding quantity in relation to the exit channel $\beta$, where i' denotes the spin of the emitted particle and I' that of the residual nucleus. Let $\ell$ and $\ell'$ denote the orbital angular momentum in the incident and outgoing channel, respectively.

The entrance channel $\alpha$ is specified by i, I, j, and $\ell$, which combine to give a resultant angular momentum J. With these additional specifications on spins, the transmission coefficient $T_{\alpha}$ is written as $T_{\alpha\ell j}$. The probability for the formation of a compound nucleus of spin J from the channel $\alpha$ is then given by

$$\sigma_{\alpha}^{(CN)J} = \pi \lambda_{\alpha}^2 (2\ell + 1) T_{\alpha\ell j}^{J} |C_{mm0}^{Jj\ell}|^2 , \tag{4-30}$$

where $C_{mm0}^{Jj\ell}$ are the well-known Clebsch-Gordan coefficients.

The details of this equation with justifications of the various terms entering in the calculations are worked out by several groups and in particular by Blatt and Beidenhorn (Ref. 12). The most important terms that enter into Equation 4-30 are $T^J_{\alpha\ell j}$, which are the transmission coefficients. These transmission coefficients are calculated by the choice of an appropriate optical potential. Once the compound nucleus is formed and the related cross section is established through Equation 4-30, it only remains to write down the cross section for the decay of the compound nucleus through the exit channel. Hauser and Fesbach (Ref. 13) and Hodgson (Ref. 14) have discussed the details of the cross section and have given

$$\sigma_{\alpha\beta}(\theta) = \Pi \lambda_\alpha^2 \sum \frac{2\ell + 1}{(2i + 1)(2I + 1)} A_J(j\ell, j', \ell'; \theta) \frac{T^J_{\alpha\ell j} T^J_{\beta\ell' j'}}{\sum_{\alpha\ell j} T^J_{\alpha\ell j}}, \quad (4\text{-}31)$$

where the $A_J$ coefficients are products of the Clebsch-Gordon and Racah coefficients and are tabulated by Blatt and Beidenhorn.

Without going into the details of the theory, which is rather well formulated, it is of interest to mention the role of optical potentials that enter into the calculation of the transmission coefficient $T^J_{\alpha\ell j}$. In any calculation using this formalism, the accuracy of the results would depend a great deal on the appropriateness of the optical well parameters.

### 4.2.4 Optical Potentials for Charged-Particle Reactions

Ever since Serber (Ref. 15) first proposed the optical model for the nuclear potential as seen by an approaching nucleon, this model has received more attention than any other form. The resemblance to a complex refractive index that appropriately explains reflection and refraction can very well explain the physical process of elastic collisions, which are similar to reflection, and to compound nonelastic collisions, which are similar to the phenomenon of refraction. There are several forms of optical potentials. In the analysis in this study, the following general form is used:

$$V(r) = Uf(r) + iWg(r) + (Us + iWs)\left(\frac{\hbar}{m_{\Pi}C}\right)^2 \frac{1}{r} \frac{dfs(r)}{dr} \bar{L} \cdot \bar{\sigma} \quad . \tag{4-32}$$

It is also found that the actual form of the potential, as well as the variable parameters occurring in Equation 4-31, are dependent on the charge and energy of the projectile. For the case of proton reactions with light nuclei and for protons of medium energy from 9 to 22 MeV, Perry (Ref. 16) has given the following values for the various parameters occurring in Equation 4-32:

$$U = 53{\cdot}3 - 0{\cdot}55E - 27 \frac{N - Z}{A} + 0{\cdot}4 \frac{Z}{A^{1/3}}$$

$$W = 3 A^{1/3}$$

$$U_s = 9{\cdot}5 \text{ for } E \geq 17$$

$$U_s = 7{\cdot}5 \text{ for } E < 17.$$

In Equation 4-32, the term corresponding to $U_s$ comes out to be

$$V_s(r) = \left(\frac{\hbar}{m_{\Pi}C}\right)^2 U_s \frac{1}{r} \frac{df(r)}{dr} \bar{L} \cdot \bar{\sigma}.$$

This is called the spin orbit term, where $\left(\frac{\hbar}{m_{\Pi}C}\right)^2 \approx 2 \cdot \text{fm}^2$ is used in the calculations, L and $\sigma$ have the usual meaning respectively, and f(r) is a form factor.

Some typical values of the various energy-dependent parameters used on the case of proton reactions are given in Table 4-1.

The mechanism and the components of the various possible types of channels in the compound-nucleus formalism are shown in Figures 4-1, 4-2, and 4-3. The cross sections for various types of reactions referenced in this discussion as well as in most literature pertaining to these reactions are shown in Figure 4-4. An ideal formalism must be able to calculate each of these components as a function of the projectile energy and spin and the channel parameters. However, the mechanism to be used for the direct reaction $\sigma(d_i)$ is definitely different from,

## TABLE 4-1. PARAMETERS FOUND IN THE ANALYSIS OF PROTON DATA WITH DIFFERENT POTENTIAL FORMS

| Comments | $U$ (MeV) | $r_U, a_U$ (fm) | $W_V$ (MeV) | $W_S$ (MeV) | $r_W, a_W$ (fm) | $V_{so}, r_{so}, a_{so}$ | $\langle\chi^2/N\rangle$ $\sigma(\theta)$ | $P(\theta)$ | $\sigma_R$ |
|---|---|---|---|---|---|---|---|---|---|
| Best fit | $54 - 0.32E + 0.4\gamma + 24\xi$ | 1.17, 0.75 | $0.22E - 2.7$ | $11.8 - 0.25E + 12\xi$ | $1.32, 0.51 + 0.7\xi$ | 6.2, 1.01, 0.75 | 12 | 7 | 6 |
| $a_W$ constant | $54 - 0.32E + 0.4\gamma + 24\xi$ | 1.17, 0.75 | $0.22E - 2.7$ | $11.8 - 0.25E + 12\xi$ | 1.32, 0.56 | 6.2, 1.01, 0.75 | 16 | 8 | 6 |
| $a_W \propto A^{\frac{1}{3}}$, $W_V \propto E$ | $54 - 0.32E + 0.4\gamma + 24\xi$ | 1.17, 0.75 | $0.15E$ | $11.8 - 0.25E + 12\xi$ | $1.32, 0.18A^{\frac{1}{3}}$ | 6.2, 1.01, 0.75 | 13 | 7 | 8 |
| $a_W \propto A^{\frac{1}{3}}$ | $54 - 0.32E + 0.4\gamma + 24\xi$ | 1.17, 0.75 | $0.22E - 2.7$ | $11.8 - 0.25E + 12\xi$ | $1.32, 0.14A^{\frac{1}{3}}$ | 6.2, 1.01, 0.75 | 12 | 7 | 8 |
| $W_V \propto \xi$ | $54 - 0.32E + 0.4\gamma + 24\xi$ | 1.17, 0.75 | $0.22E - 2.7 + 1.4\xi$ | $11.8 - 0.25E + 12\xi$ | 1.32, 0.56 | 6.2, 1.01, 0.75 | 14 | 7 | 7 |
| $W_S \propto A^{\frac{1}{3}}$ | $54 - 0.32E + 0.4\gamma + 24\xi$ | 1.17, 0.75 | $0.22E - 2.7$ | $0.77A^{\frac{1}{3}} - 0.28E$ | $1.27, 0.51 + 0.7\xi$ | 6.2, 1.01, 0.75 | 20 | 9 | 10 |
| $r_S = r_U = 1.17$ | $54 - 0.32E + 0.4\gamma + 24\xi$ | 1.17, 0.75 | $0.22E - 2.7$ | $11.8 - 0.25E + 12\xi$ | $1.32, 0.51 + 0.7\xi$ | 5.9, 1.17, 0.60 | 16 | 9 | 6 |
| $V_s \propto E$ | $54 - 0.32E + 0.4\gamma + 24\xi$ | 1.17, 0.75 | $0.22E - 2.7$ | $11.8 - 0.25E + 12\xi$ | $1.32, 0.51 + 0.7\xi$ | $9.0 - 0.1E$, 1.01, 0.75 | 13 | 7 | 6 |
| $U \propto E^2$ | $59.7 - 0.47E + 0.9E^2 + 0.4\gamma + 24\xi$ | 1.15, 0.76 | $0.22E - 2.7$ | $11.8 - 0.25E + 12\xi$ | $1.32, 0.51 + 0.7\xi$ | 6.2, 1.01, 0.75 | 17 | 8 | 7 |
| Best $r_U = 1.12$ | $58.8 - 0.32E + 0.4\gamma + 24\xi$ | 1.12, 0.78 | $0.22E - 2.7$ | $11.8 - 0.25E + 12\xi$ | $1.32, 0.51 + 0.7\xi$ | 6.2, 0.98, 0.75 | 15 | 7 | 8 |
| Best $r_U = 1.22$ | $50 - 0.32E + 0.4\gamma + 24\xi$ | 1.22, 0.72 | $0.22E - 2.7$ | $11.8 - 0.25E + 12\xi$ | $1.32, 0.51 + 0.7\xi$ | 6.2, 1.06, 0.68 | 15 | 7 | 8 |
| $U_1 = 0, r_U \propto \xi$ | $58.5 - 0.32 + 0.4\gamma$ | $1.11 + 0.33\xi$, 0.76 | $0.22E - 2.7$ | $11.8 - 0.25E + 12\xi$ | $1.32, 0.51 + 0.7\xi$ | 6.2, 1.01, 0.75 | 13 | 8 | 8 |
| $U_1 = 0, a_U \propto \xi$ | $56 - 0.24E + 0.4\gamma$ | $1.15, 0.66 + 1\xi$ | $0.22E - 2.7$ | $11.8 - 0.25E + 12\xi$ | $1.32, 0.51 + 0.7\xi$ | 6.2, 1.01, 0.75 | 14 | 8 | 8 |
| $V_c = 0$ | $57.3 - 0.32E + 28\xi$ | 1.17, 0.75 | $0.22E - 2.7$ | $11.8 - 0.25E + 12\xi$ | $1.32, 0.51 + 0.7\xi$ | 6.2, 1.01, 0.75 | 14 | 8 | 6 |
| $V_c = 0.3$ | $54.9 - 0.32E + 0.3\gamma + 25\xi$ | 1.17, 0.75 | $0.22E - 2.7$ | $11.8 - 0.25E + 12\xi$ | $1.32, 0.51 + 0.7\xi$ | 6.2, 1.01, 0.75 | 12 | 7 | 6 |
| $V_{cc} = 0.84$ * | $55.2 - 0.32E + 0.27\gamma + 24\xi$ | 1.17, 0.75 | $0.22E - 0.18\gamma - 1.4$ | $10.2 - 0.25E + 0.21\gamma + 12\xi$ | $1.32, 0.51 + 0.7\xi$ | 6.2, 1.01, 0.75 | 12 | 7 | 6 |
| $r'_W = 1.22$, $a'_W = 0.72$ ** | $54 - 0.32E + 0.27\gamma + 24\xi$ | 1.17, 0.75 | $0.22E - 2.7$ | $11.8 - 0.25E + 12\xi$ | $1.32, 0.51 + 0.7\xi$ | 6.2, 1.01, 0.75 | 13 | 7 | 6 |
| $U_1 = 9$ *** | $56 - 0.32E + 0.4\gamma$ | 1.17, 0.75 | $0.22E - 2.7$ | $11.8 - 0.25E + 12\xi$ | $1.32, 0.51 + 0.7\xi$ | 6.2, 1.01, 0.75 | 14 | 8 | 7 |

* Variable Coulomb energy term added to all energy-dependent strengths; i.e., incident proton energy $E$ replaced by an effective energy $E - V_{cc}Z/A^{\frac{1}{3}}$ with $V_{cc}$ a search parameter.

** Separate geometry used for volume imaginary potential with $W(r) = -W_V f(r, r'_W, a'_W) + W_S 4a_W(\mathrm{d}/\mathrm{d}r)[f(r, r_W, a_W)]$.

*** Volume real symmetry term replaced by surface form: $U_1^S(r) = -U_1\xi 4a_U(\mathrm{d}/\mathrm{d}r)[f(r, r_U, a_U)]$.

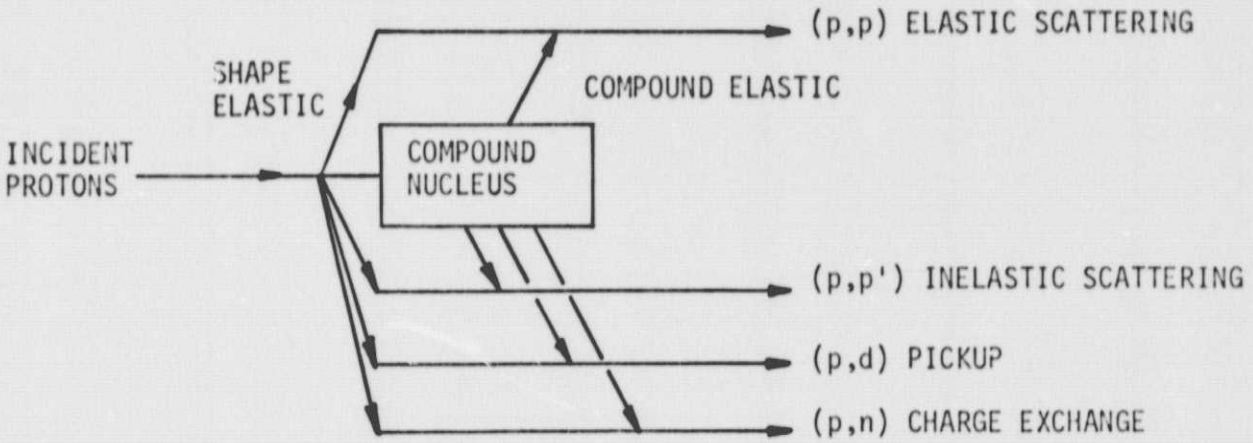


FIGURE 4-2. SCHEMATICS OF VARIOUS CHANNELS ENTERING IN PROTON REACTIONS

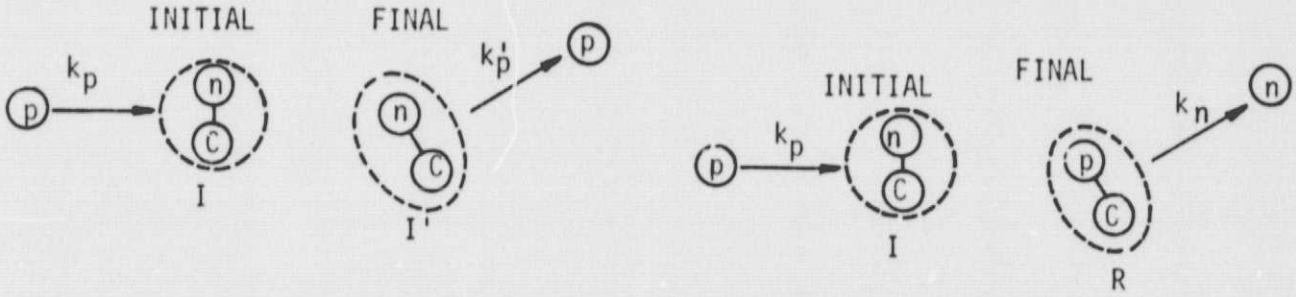


a. INELASTIC SCATTERING

b. KNOCKOUT REACTION

FIGURE 4-3. INELASTIC SCATTERING AND KNOCKOUT REACTION

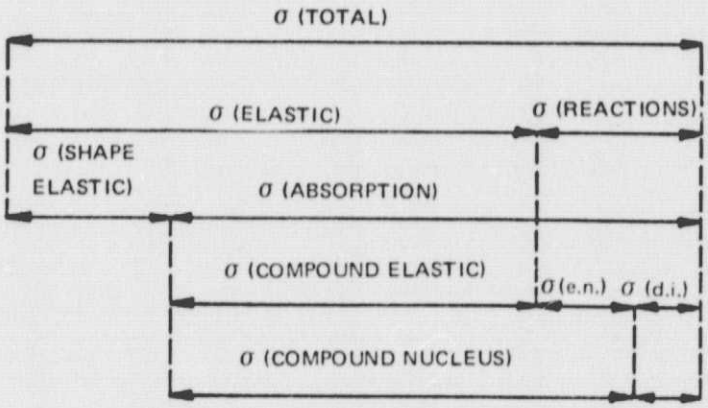


FIGURE 4-4. COMPONENTS OF THE TOTAL CROSS SECTION

for example, the Hauser-Fesbach formalism, which will be used in this discussion for the evaluation of inelastic cross sections.

### 4.2.5 Hauser-Fesbach Calculations

Based on the formalism developed in the previous section and adopting ABACUS II (Ref. 17), the inelastic cross sections are calculated for $_8O^{16}$, $_7N^{14}$, and $_6C^{12}$. However, the following modification has been made in the existing ABACUS II. The coulomb subroutine has been replaced by the more recent Manchester Code (Ref. 18). The Coulomb wave functions $F_i(\eta,\rho)$ and $G_\ell(\eta,\rho)$ and their respective first derivations are determined from the solution to

$$\frac{d^2 U_\ell}{d\rho^2} + \left[1 - \frac{2\eta}{\rho} - \frac{\ell(\ell+1)}{\rho^2}\right] G_\ell = 0 \quad ,$$

where

$$\rho = \left(2 \mu E \frac{r^2}{\hbar^2}\right)^{1/2}$$

$$\eta = \frac{Z_1 Z_2 e_2}{\hbar^2 k} \quad ,$$

where $Z_1e$ is the charge of the projectile and $Z_2e$ that of the target, k is the wave number, and E is the center-of-mass energy. The program for the coulomb wave function can be incorporated into the ABACUS II or may be run separately and the relevant data put into the calculation to be made for charged particle reactions.

The intrinsic parameters of the target nucleus for oxygen 16 are shown in Figure 4-5. The various parameters that enter into the optical potential well used in the HF calculation are given in Table 4-1. The energy dependence of these parameters is clear from Table 4-1. Table 4-2 gives a comparison of these parameters at a fixed proton energy of 16·3 MeV. ABACUS II in conjunction with the Manchester Code strictly calculates only the (p,p') reaction cross sections. There is no provision in the formalism developed to handle any nonelastic channels leading to charge exchange or any other type of inelastic process.

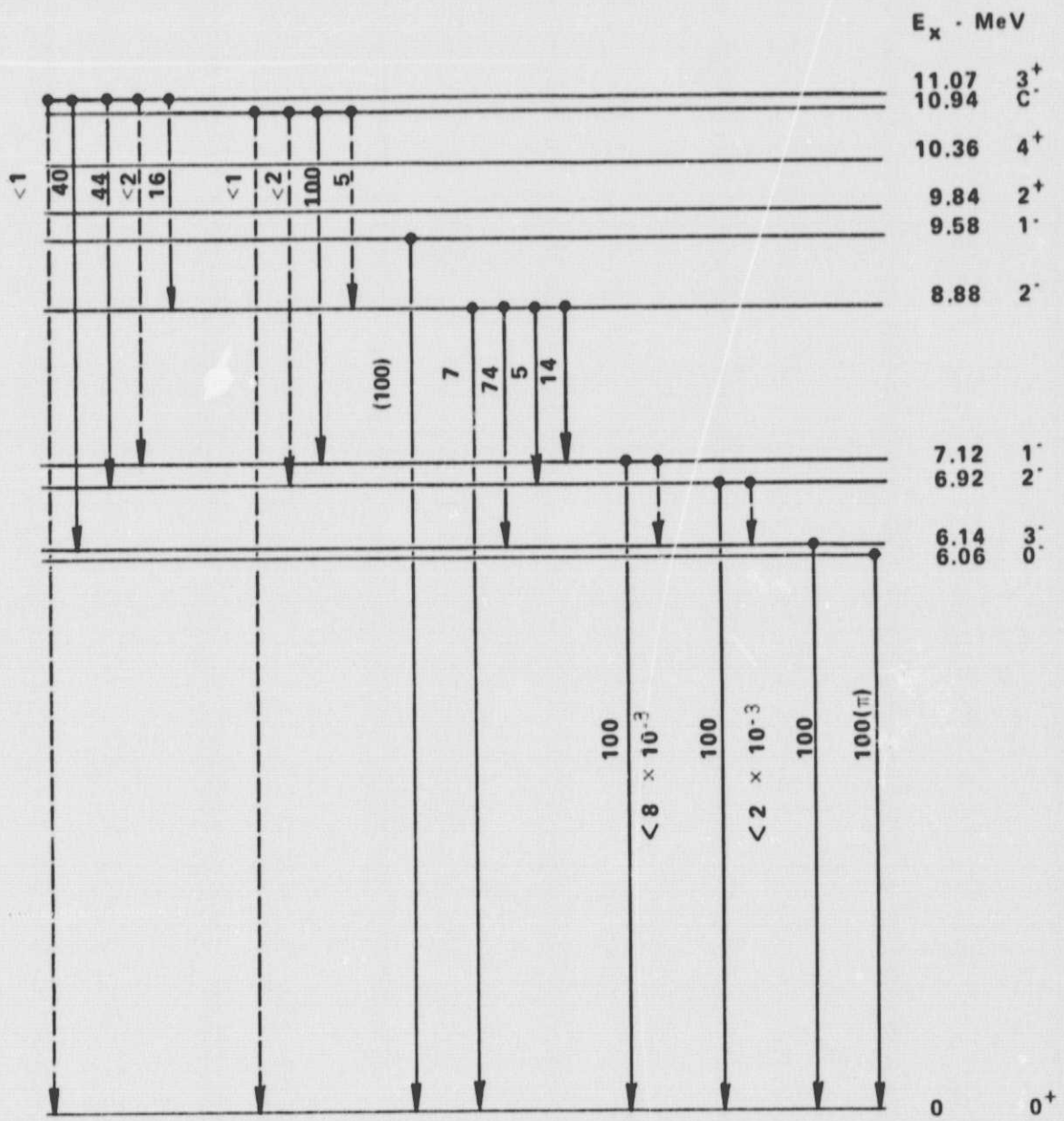


FIGURE 4-5. GAMMA-RAY TRANSITIONS IN $O^{16}$

TABLE 4-2. PROTON INELASTIC CROSS SECTION FOR $_8O^{16}$

| $E_L$ (MeV) \ $E_p$ (MeV) | σ (p,p') in mb | | | | |
|---|---|---|---|---|---|
| | 11 | 12 | 13 | 14 | 15 |
| 6·06 | 16·7 | 18·2 | 29·8 | 47·3 | 56 |
| 6·14 | 12.3 | 16·4 | 25·6 | 31·6 | 36·5 |
| 6·92 | 12·2 | 11·2 | 17·3 | 22·4 | 25·8 |
| 7·12 | 9·7 | 9·9 | 12·6 | 16·2 | 18·8 |
| 8·88 | 6·2 | 6·8 | 10·9 | 16·2 | 16·5 |
| 9·58 | 3·3 | 3·9 | 6·8 | 9·7 | 10·3 |
| 9·84 | 9·6 | 9·9 | 16·6 | 21·4 | 19·7 |
| 10·36 | 12·2 | 13·1 | 19.9 | 27·3 | 30·1 |
| 10·94 | 0·0 | 0·2 | 1·0 | 1·5 | 2·0 |
| 11·07 | 6·8 | 6·9 | 9·6 | 16·2 | 12·9 |

The cross sections to excite each of the states are given in Table 4-3 as a function of $E_p$, where $E_p$ denotes the proton energy.

Tables 4-4 and 4-5 give similar calculations for $_7N^{16}$ and $_6C^{12}$; Figures 4-6 and 4-7 show the respective transitions of interest.

4.2.6 Discussion of Results

The results of the calculations carried out by adopting the modified ABACUS Code with the introduction of the Coulomb routine through the Manchester Code are given in Tables 4-2, 4-3, and 4-4 for $_6C^{12}$, $_7N^{16}$, and $_8O^{16}$ nuclei and for proton energies from 11 to 15 MeV. The parameters of the excited states entering the computation are shown in the respective local schemes of these nuclei in Figures 4-5, 4-6, and 4-7, respectively. The calculation is clearly dependent on the optical potential parameters chosen. Bechetti and Greenless (Kef. 21) have

TABLE 4-3. PROTON INELASTIC CROSS SECTION FOR $_7N^{14}$

| $E_L$ (MeV) \ $E_p$ (MeV) | σ(p,p') in mb | | | | | | |
|---|---|---|---|---|---|---|---|
| | 11 | 12 | 13 | 14 | 15 | 16·5* | 16·6** |
| 2·31 | 8·8 | 6·9 | 5·7 | 7·9 | 6·6 | 2·9 | 3·2 |
| 3·94 | 18·2 | 23·4 | 18·9 | 16·9 | 22·3 | 17·5 | 18·5 |
| 4·91 | 5·3 | 4·3 | 6·1 | 4·6 | 4·4 | 3·3 | 1·8 |
| 5·1 | 38·26 | 29·0 | 32·1 | 29·6 | 26·9 | 16·0 | 19·0 |
| 5·69 | 18·2 | 16·6 | 11·96 | 16·9 | 16·0 | 8·8 | 8·7 |
| 5·83 | 56·9 | 43·1 | 32·7 | 45·38 | 40·1 | 19·6 | 19·2 |
| 6·23 | 10·28 | 13·7 | 11·59 | 16·7 | 13·8 | 5·8 | 1·7 |
| 6·60 | 10·1 | 16·8 | 11·9 | 16·9 | 13·3 | 6·0 | 5·9 |
| 7·03 | 19·4 | 15·4 | 23·2 | 17·2 | 26·9 | 23·6 | 27·9 |
| 7·4 | 10·2 | 8·4 | 11·7 | 9·4 | 9·6 | | |
| 7·6 | 37·7 | 28·7 | 32·7 | 29·4 | 27·4 | | |
| 7·96 | 10·65 | 16·1 | 13·4 | 17·4 | 16·4 | | |
| 8·06 | 5·7 | 8·4 | 7·2 | 9·3 | 8·9 | | |
| 8·62 | 1·8 | 2·6 | 2·3 | 3·0 | 2·8 | | |

*From Reference 19

**From Reference 20

TABLE 4-4. PROTON INELASTIC CROSS SECTION FOR $_6C^{12}$

| $E_L$ (MeV) \ $E_p$ (MeV) | σ(p,p') in mb | | | | |
|---|---|---|---|---|---|
| | 11 | 12 | 13 | 14 | 15 |
| 4·433 | 31·8 | 51·2 | 59·6 | 64·7 | |
| 7·65 | 6·6 | 7·0 | 8·2 | 10·1 | |
| 9·63 | 20·0 | 25·0 | 27·6 | 31·7 | |
| 10·10 | 1·6 | 2·2 | 4·2 | 4·6 | |
| 12·73 | 3·9 | 4·9 | 5·9 | 6·5 | |

TABLE 4-5. OPTICAL MODEL PARAMETERS USED IN THE CURRENT CALCULATION

| OPTICAL MODEL PARAMETERS* | $_6C^{12}$ | $_7N^{14}$ | $_8O^{16}$ |
|---|---|---|---|
| VRC | 58·2 | 50·4 | 51·62 |
| VIM | 19·9 | 3·0 | 3·0 |
| R1 | 2·747 | 3·05 | 1·25 |
| A1 | 0·4 | 0·68 | 0·58 |
| RC | 2·74 | 0· | 1·25 |
| R2 | 2·74 | 3·05 | 1·25 |
| A2 | 0·25 | 0·7 | 0·6 |
| SO-REAL | 6·0 | 7·0 | 6·9 |

*The various symbols used correspond to the description in ABACUS II

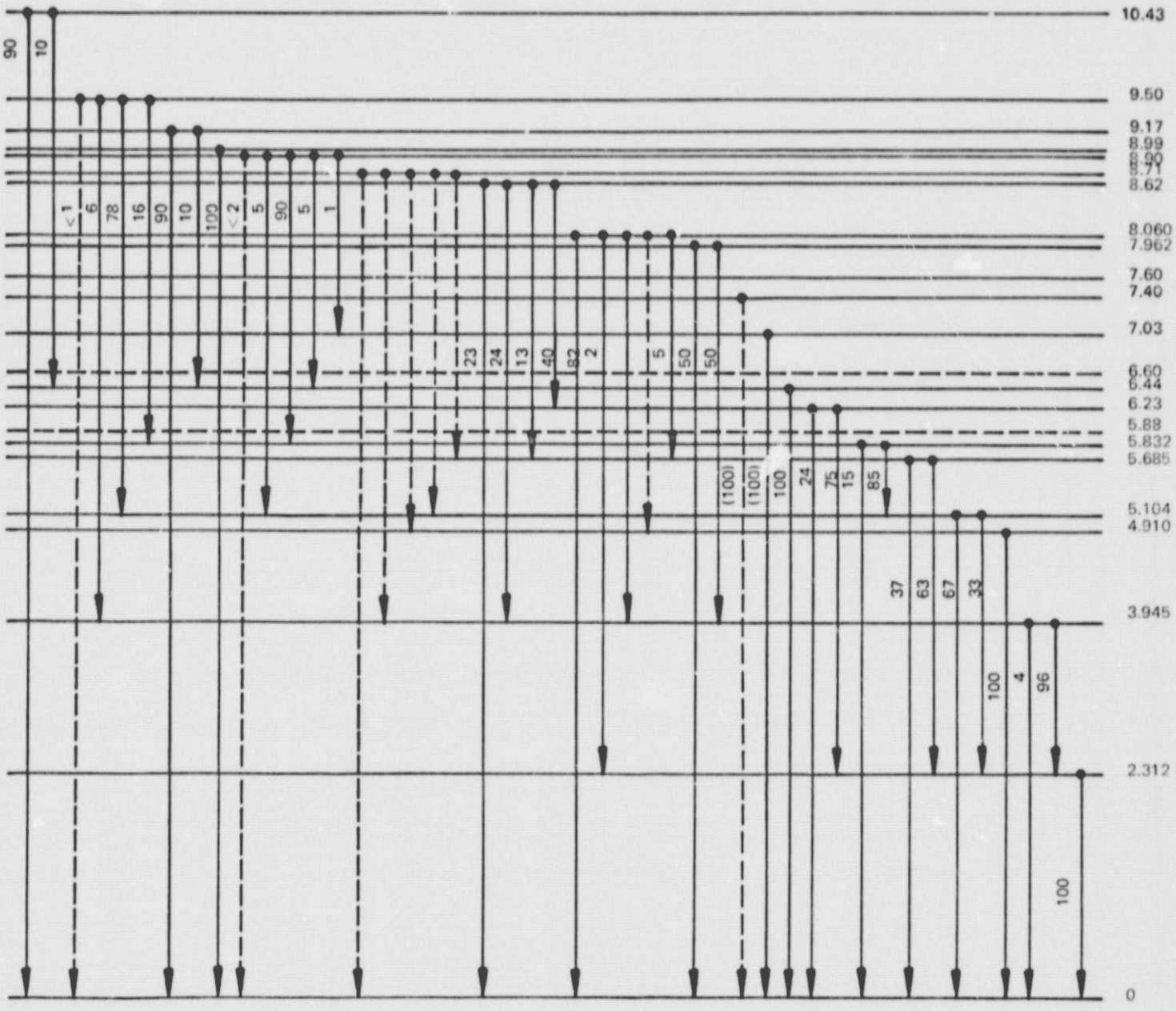


FIGURE 4-6. ENERGY STATES OF $_7N^{14}$

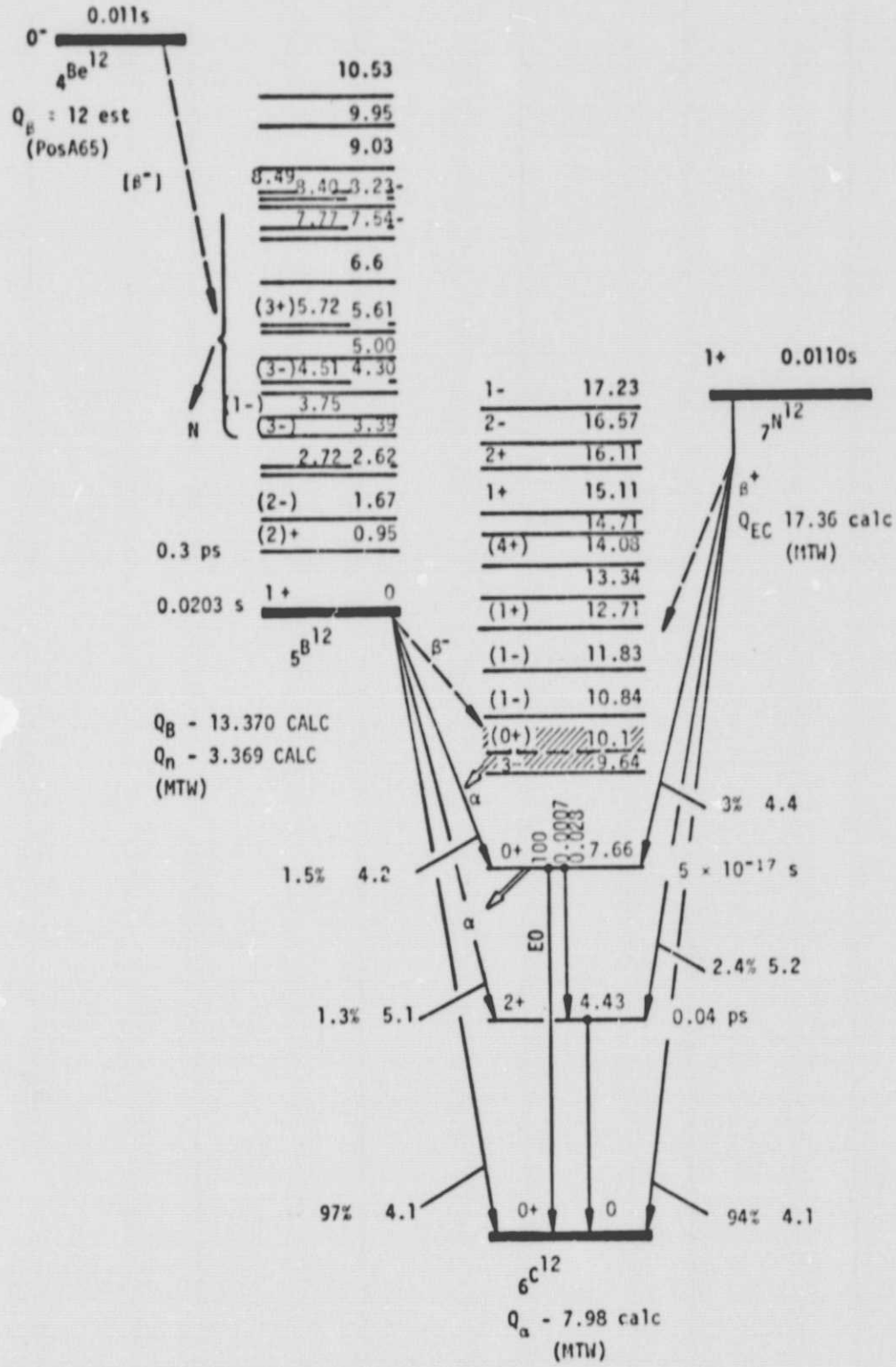


FIGURE 4-7. ENERGY STATES OF $_6C^{12}$

carried out extensive analyses of potential parameters for proton energies less than 50 MeV. The most complete analyses have been carried out by Perry (Ref. 16) for proton elastic scattering from 9 to 22 MeV. A summary of these analyses is shown in Table 4-1, which is adopted from Hodgson (Ref. 14). The values of the various optical model parameters defined in ABACUS are given in Table 4-2.

The calculated values of the inelastic cross sections for each of the states of $_7N^{14}$ at a proton energy of 14 MeV, as given in Table 4-3, compare favorably with reported results. However, there is some degree of disagreement because the inelastic processes that open up due to other types of reactions are not considered in the formalism. Therefore, at best this technique can calculate only the inelastic cross sections for the case in which such particle emission cross sections are negligible.

In the case of light nuclei of interest here, for energies of about 14 MeV, other inelastic channels can become available. Therefore, it is found to be necessary to incorporate a theory for handling such situations. Such a formalism is discussed in the next section.

4.2.7 Coupled-Channel Formalism

The application of compound-nucleus formalism with no regard for exit channels leading to emission of different particles is, at best, rather a crude approximation when the projectile energy is of the order of or higher than the observed Q value for a particular reaction. However, as mentioned earlier, if such reactions are to be taken into consideration, other theoretical formalism should be developed. The variation of cross section with the energy of the projectile as well as reported shape of the angular distributions lead to the conclusion that, at energies of interest here, the contribution from the compound state to other channels is not negligible. Thus, for example, in Table 4-3 the calculated value and the measured value of inelastic cross sections of $_7N^{14}$ at an incident proton energy of 16.5 MeV are not in agreement. The calculation employing the Hauser-Fesbach formalism will give the compound inelastic cross section only. The direct inelastic cross section

leading to inelastic channels, such as (p,α) reactions, will have to be handled by adopting the macroscopic and microscopic coupled-channel calculation as developed in the Oregon State University coupled-channel code (Ref. 22).

4.2.8 Coupled Channel Theory

In a simple situation one can assume that a spinless particle reacts with a nucleus and raises the nucleus to a series of spinless excited states.

Let the kinetic energy operator corresponding to the incident particle be presented by

$$T = -\frac{\hbar^2}{2m} \nabla_r^2 \quad ,$$

the nuclear Hamiltonian be given by $H(\xi)$, and the interaction potential between the projectile and the nucleus be represented by $V(r, \xi)$. The Schrödinger equation pertaining to this situation can be written as

$$[T - V(r, \xi) + H(\xi)]\, \Psi(r, \xi) = E\Psi(r, \xi) \quad . \tag{4-33}$$

The nuclear states must be eigen states of the nuclear Hamiltonian so that these states, $\chi_a(\xi)$, should satisfy the relation

$$H(\xi)\, \chi_a(\xi) = \epsilon_a \chi_a(\xi) \quad . \tag{4-34}$$

The eigen functions, $\chi_a(\xi)$, must form a complete orthonormal set, and hence the wavefunctions can be expanded in terms of this orthonormal set and can be expressed as

$$\Psi(r, \xi) = \sum_a \Psi_a(r)\, \chi_a(\xi) \tag{4-35}$$

It now becomes possible to make use of Equations 4-34 and 4-35 in Equation 4-33. By substituting Equations 4-34 and 4-35 in Equation 4-33 and after multiplying on the left by $\chi_a^*(\xi)$, the resulting function is integrated over the entire nuclear coordinates to obtain

$$\int \chi_a^*(\xi)\ [T - V(r, \xi) + H(\xi)] \sum_a \Psi_a(r)\ \chi_a(\xi)\ d\xi$$

$$= E \int \chi_a^*(\xi) \sum_a \Psi_a(r)\ \chi_a(\xi)\ d\xi \quad , \tag{4-36}$$

$$\int \chi_a^*(\xi)\ (T - V) \sum_a \Psi_a(r)\ \chi_a(\xi)\ d\xi$$

$$+ \int \chi_a^*(\xi)\ \epsilon_a\ \chi_a(\xi) \sum_a \Psi_a(r)\ \chi_a(\xi)\ d\xi$$

$$= E \int \chi_a^*(\xi) \sum_a \Psi_a(r)\ \chi_a(\xi)\ d\xi \quad ,$$

and

$$[(T - E + \epsilon_a) \int \chi_a^*(\xi) \sum \Psi_a(r)\ \chi_a(\xi)\ d\xi]$$

$$= \int \chi_a^* V \sum_a \Psi_a(r)\ \chi_a(\xi)\ d\xi$$

$$= \sum \left( \int \chi_a^* V\ \chi_a\ d\xi \right) \Psi_a$$

$$= \sum V_{aa'}\ \Psi_a \quad . \tag{4-37}$$

In Equation 4-37

$$V_{aa'}(r) = \int \chi_a'^*(\xi)\ V(r, \xi)\ \chi_a'(\xi)\ d\xi \quad .$$

The usual technique of expanding into partial waves can be used at this stage, and thus one writes

$$\psi_a(\bar{r}) = \sum \frac{U_a(r)}{r} Y_L^M(\theta,\phi) \quad . \tag{4-38}$$

This expansion is substituted into Equation 4-37, then multiplied on the left by $Y_L^{M*}$, and then integrated over $\theta$ and $\phi$ to obtain

$$\int Y_L^{M*}(\theta,\phi)\,(T - E_\alpha) \sum \frac{U_a(r)}{r} Y_L^M(\theta,\phi)\, d\Omega$$

$$= \int Y_L^{M*}(\theta,\phi) \sum_{\substack{a'=1 \\ LM}}^{N} V_{aa'}(r) \frac{U_a(r)}{r} Y_L^M(\theta,\phi)\, d\Omega \quad . \tag{4-39}$$

Here

$$E_\alpha = E - \epsilon_a = \frac{\hbar k^2}{2m} \quad .$$

Let

$$W_{aa'}(r) = \frac{2m}{\hbar^2} \sum_{LM} \int Y_L^{M*}(\theta,\phi)\, V_{aa'}(r)\, Y_L^M(\theta,\phi)\, d\Omega \quad . \tag{4-40}$$

Then Equation 4-39 can be written as

$$\left[T - \frac{\hbar k^2}{2m} - V\right] U_a(r) = \sum W_{aa'}(r)\, U_a(r) \quad .$$

This equation can be written in the form

$$\left[\frac{\hbar^2}{2m}\frac{d^2}{dr^2} - \frac{\hbar^2 \ell\,(\ell+1)}{2mr^2} - V_{O_{pr}} - V_{S.O} - V_{coul} + E - E_n\right] U_a(r)$$

$$= \sum V_{int}\, U_a(r) \quad . \tag{4-41}$$

Equation 4-41 couples all the elastic channels with the inelastic channels.

The equation can be numerically solved adapting the coupled-channel code developed by Oregon State University. It is of interest to pursue this aspect of the problem to obtain a meaningful result for the various inelastic cross sections, particularly those leading to the particle emission channels. However, it is expected that such a study would consume several months of effort.

## 4.3 CONCLUSIONS AND RECOMMENDED PLAN FOR FURTHER STUDY

The coupled-channel code as developed by Oregon State University is a rather extensive analytical technique. The original code was developed for the CDC 6600 assembly. It has been possible in this effort to study the applicability of this formalism as an improvement on the possible inelastic cross section calculations. It is strongly felt that ABACUS II in conjunction with the Manchester Coulomb Code and the coupled-channel code can lead to a more extensive and complete analysis of the charged-particle reaction in the case of light nuclei. The coupled-channel code has been adapted for the Univac 1108 assembly and is ready to be put into operation should such an investigation be considered of interest.

# 5. REFERENCES


1. "Nucleus-Nucleus Collision at Cosmic Ray Energies", Teledyne Brown Engineering Report No. SE-SSL-1370, August 1971

2. E. G. Stassinopoulos, "World Maps of Constant B, L and Flux Contours", NASA SP-3054, 1970

3. J. P. Lavine and J. I. Vette, "Models of the Trapped Radiation Environment, Vol. VI: High Energy Protons", NASA SP-3024, 1970

4. L. E. Peterson, Journal of Geophysical Research, Vol. 70, p. 1762, 1965

5. S. V. Golenetskii, Astrophysical Letters, Vol. 9, p. 69, 1971

6. C. S. Dyer and G. E. Morfill, Astrophysics and Space Science, Vol. 14, p. 243, 1971

7. G. J. Fishman, "Proton-Induced Radioactivity in NaI(Tℓ) Scintillation Detectors", Teledyne Brown Engineering Report No. SE-SSL-1497, 1972

8. G. J. Fishman, The Astrophysical Journal, Vol. 171, p. 163, 1972

9. G. Rudstam, Zeitschrif für Naturforschung, Vol. 21a, p. 1027, 1966

10. J. Ladenbauer and L. Winsbert, Physical Review, Vol. 119, p. 1368, 1960

11. "Skylab Neutron Environment Experiment [Science Demonstration SD-34 (TV108)]", Teledyne Brown Engineering Report No. EE-SSL-1802, April 1974

12. J. M. Blatt and L. C. Beidenhorn, Rev. Mod. Phys., Vol. 24, p. 258, 1952

13. W. Hauser and H. Fesbach, Phys. Rev., Vo.. 87, No. 2, p. 366, 1972

14. P. E. Hodgson, Nuclear Reactions and Nuclear Structure, Clarendon Press, Oxford, pp. 285-319, 1971

15. R. Serber, Phys. Rev., Vol. 72, 1008, 1961

16. F. G. Perry, Phys. Rev., Vol. 131, p. 745, 1963

17. E. H. Auerbach, "ABACUS II - Program Operation and Input Description", BNLbsb2, 1962

18. A. R. Barnett, D. H. Feng, J. W. Steed, and L. J. Goldfarb, Comp. Phys. Comm., Vol. 8, p. 377, 1974

19. L. F. Hansen, S. M. Grimes, J. L. Kammerdiener, and V. A. Madsen, Phys. Rev., Vol. 8 C, No. 6, p. 2072, 1973

20. T. H. Curtis and H. F. Lutz, Nuclear Phys., A165, Vol. 9, 1971

21. F. D. Bechett and G. W. Greenless, Phys. Rev., Vol. 182, p. 1190, 1969

22. Oregon State Coupled Channel Code, Oregon State University